

Effect of TiO₂ doping on microstructural properties of Al₂O₃-based single crystal ceramics

Serkan Abali*

Can Vocational College, Canakkale Onsekiz Mart University, Canakkale, 17400, Turkey

Powders of Al₂O₃-TiO₂ containing, 48 and 40% TiO₂ by weight were formed into single crystals with a Verneuil furnace at 2088 K. Raman spectroscopy was used to determine the phase composition of the samples solidified from the Al₂O₃-TiO₂ powder. The resulting β-Al₂TiO₅-Al₆Ti₂O₁₃, β-Al₂TiO₅-Al₂O₃ single crystals were probed with micro hardness assays, scratch test analyses, atomic force microscopy (AFM), scanning electron microscopy (SEM), thermal expansion and four-point bending tests. It was observed that the alumina-tialite single crystal retained a composition of Al₂O₃-TiO₂ containing 60% Al₂O₃ by weight and displayed optimum properties.

Key words: Alumina, Alumina-tialite, Single crystal, Microstructure.

Introduction

Eutectic ceramics are important materials because they have superior features, such as high bending and creep strengths [1-3]. Recently, fabrication methods of eutectic ceramics have been substantially researched. Eutectic ceramics are generally fabricated by cooling a melt with a eutectic composition [4-6]. Aluminium titanate, Al₂TiO₅, is known to be a promising candidate material for application in the fields of refractory and engine components because of its low thermal expansion, excellent thermal shock resistance, and low thermal conductivity [7]. The addition of Al₂TiO₅ to Al₂O₃ improves the fracture toughness of alumina due to the enhancement of the local residual stress induced by the difference of thermal expansion coefficients between Al₂O₃ and Al₂TiO₅ [8, 9].

Considering the toughening mechanisms in alumina-based composites materials, it is important to control the microstructure of the matrix as well as the morphology of the second-phase [10].

In addition to the importance of the primary phases in eutectic structures, crack deflection at micro-cracked regions can be more pronounced due to the shape of the reinforcing phase rods [11]. In this sense, Al₂O₃-Al₂TiO₅ composites offer unique opportunities for toughening due to the high thermal expansion anisotropy of the pseudobrookite structure (α_a 25-1000 °C = $10.9 \times 10^{-6} \text{C}^{-1}$, α_b 25-1000 °C = $20.5 \times 10^{-6} \text{C}^{-1}$, α_c 25-1000 °C = $-2.7 \times 10^{-6} \text{C}^{-1}$) and its mismatch with alumina (α_a 25-1000 °C = $7.7 \times 10^{-6} \text{C}^{-1}$, α_a 25-1000 °C = $8.6 \times 10^{-6} \text{C}^{-1}$ in the hexagonal system) [11].

As reported elsewhere [12, 13], the Al₂O₃-Al₂TiO₅ eutectic

specimens were made of two aluminium titanate phases, Al₆Ti₂O₁₃ and Al₂TiO₅. Goebbels and Bostroem published an extended abstract describing the solidification of Al₆Ti₂O₁₃ and proposed a first structure for this new phase. The Al₆Ti₂O₁₃ structure was derived from the Al₂TiO₅ pseudobrookite structure [14].

The purpose of this study, with different amounts of additives, obtained in TiO₂, Al₂O₃-based single crystals with optimized properties is to determine the microstructural properties.

Experimental

Crystals weighing 250 g were obtained by the flame fusion method with a melting temperature of 2088 K, a growth rate of 5 mm.h⁻¹ and a cooling rate of 313.15 K.h⁻¹. With respect to the phase diagram in Fig. 1 [15], high

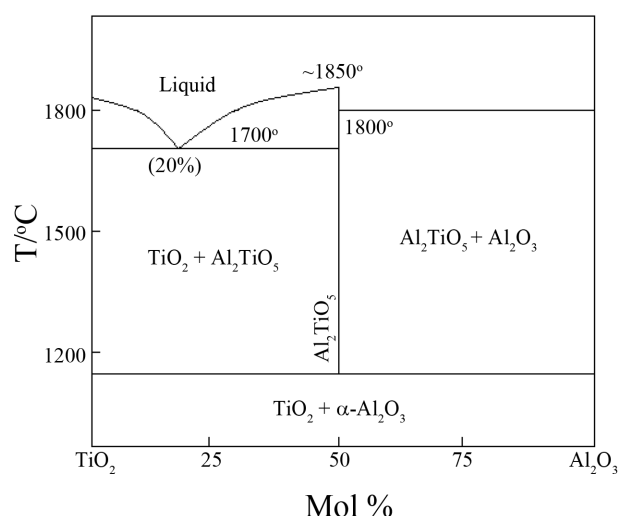


Fig. 1. Al₂O₃-TiO₂ phase diagram proposed by Goldberg in 1968 [15].

*Corresponding author:
 Tel : +90-286-416-7705
 Fax: +90-286-416-7706
 E-mail: sabali@comu.edu.tr

purity (99.9%) Al_2O_3 and TiO_2 (Kale Mining, Turkey) were homogenized in a ball mill to a size of 0.3 micrometre. The mole fraction of the eutectic composition is $\text{Al}_2\text{O}_3/\text{TiO}_2 = 52/48; 60/40$. Since pulverizing the powder extended the melting time, the powder was formed into granules by dehumidification with calcinations at 1173 K instead of sintering. The powder was then fed into the funnel of a Verneuil furnace (YTU-Ceramic Laboratory, Turkey).

The flow of powder at the desired concentrations was manipulated by the flow of gas into the central tube and the vibrator. The falling powder precipitated on the cone-shaped stick during sintering. When the flow of gas increased, the heat of the flame increased. The surface of the sinter cone was melted, and a seed for crystallization was produced. The flame was gradually increased while controlling the flow concentration. The gas flow and flame temperature were maintained while the flow concentration increased.

To achieve high quality crystals, all the parameters must be stable and the crystals must be grown slowly. For example, an unstable gas pressure with a strong flame produces dislocations in the crystal.

A sapphire seed crystal was used for growth initiation. The flow rate of hydrogen fuel was $60 \text{ l}\cdot\text{minute}^{-1}$, and the flow rate of oxygen was $45 \text{ l}\cdot\text{minute}^{-1}$. The H_2 pressure was maintained at 1.2 bar, and the O_2 pressure was kept at 10 bar. Although the amounts of H_2 and O_2 gases were varied to control crystal growth, the ratio of H_2/O_2 was 2/1 at all times.

Raman spectroscopy (Confocal laser raman and photoluminescence micro spectrometer) was used to acquire information about the phase composition of the as-grown $\beta\text{-Al}_2\text{TiO}_5\text{-Al}_2\text{O}_3$, $\beta\text{-Al}_2\text{TiO}_5\text{-Al}_6\text{Ti}_2\text{O}_{13}$ crystals. The hardness of grown crystals and polycrystalline $\beta\text{-Al}_2\text{TiO}_5\text{-Al}_2\text{O}_3$ were measured using a Vickers micro hardness instrument at room temperature. A load of 1.9 N was applied for 10 s (HVS 1000). Scratch tests on grown crystal were conducted using a micro scratch tester (CSM) at room temperature and a relative humidity level range of $25\% \pm 2\%$. AFM images of surface topographies on the molecular scale (Q Scope) and SEM micrographs of microstructures (Jeol-6335F) were taken. The temperature dependent expansion behavior of grown crystals was also examined (Netszch dilatometer DIL 402C/3/F). The dimensions of the flexural test grown crystals and polycrystals were $3 \times 4 \times 30 \text{ mm}$ with a 20 mm span and they were mechanically tested at 1400 °C using a four-point bending device in a universal testing machine (Zwick UTM), at a crosshead speed of $0.5 \text{ mm}\cdot\text{minute}^{-1}$.

Results and Discussion

Fig. 2 shows the mineral analysis of the $\beta\text{-Al}_2\text{TiO}_5\text{-Al}_6\text{Ti}_2\text{O}_{13}$ (AT48), $\beta\text{-Al}_2\text{TiO}_5\text{-Al}_2\text{O}_3$ (AT40) single crystals. AT40 phase compositions were determined using the one sharp peak obtained at 748 cm^{-1} wavelength. The sharp, intense peak confirms the quality of the AT40 phase. The broad and asymmetric nature of this peak is typical of the Raman active mode specially observed from the talite structure. The spectrum is dominated by the presence

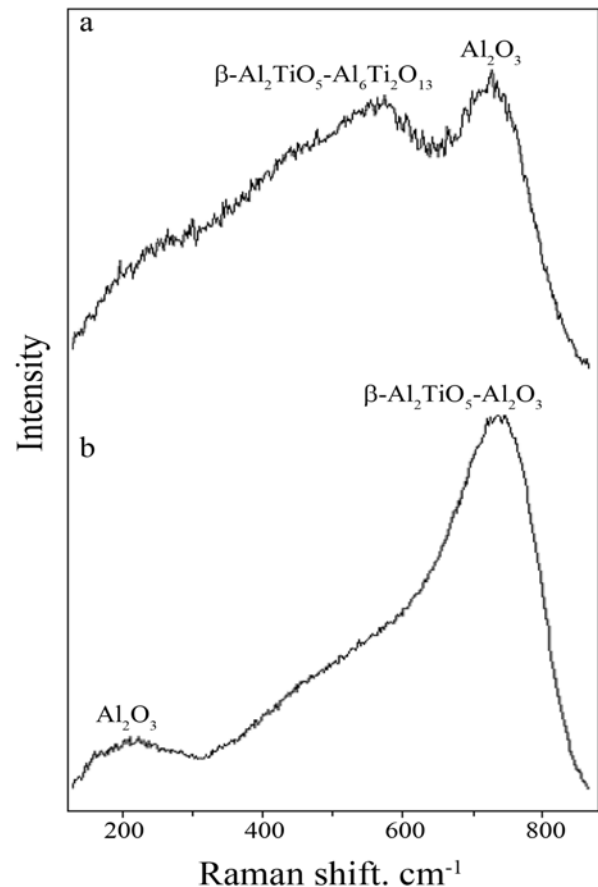


Fig. 2. Raman spectra of the AT40 and AT48 crystal. With the highest peak intensity AT40 crystals in terms of quantity and quality compared with the AT48 crystal provides positive results.

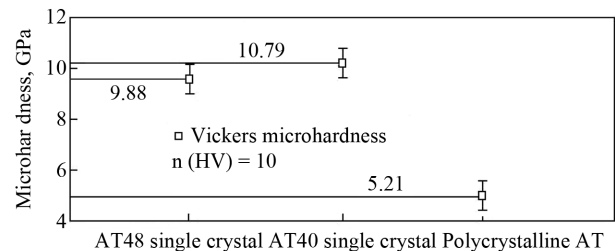


Fig. 3. Comparison of the microhardnesses of AT40, polycrystalline samples and AT48 crystal. Vickers microhardness are in the ranges of $10.79 \pm 0.8 \text{ GPa}$, $9.88 \pm 0.4 \text{ GPa}$ and $5.21 \pm 0.6 \text{ GPa}$ for AT40, AT48 single crystals and polycrystalline AT40.

of a strong peak located at 748 cm^{-1} followed by a peak (Al_2O_3) at 226 cm^{-1} in the low wavelength number region. Increasing the amount of the TiO_2 phase the AT48 crystal gave a peak at 546 cm^{-1} obtained wavelength with an intensity lower than that of the remaining AT40 phase. There is only one peak at 744 cm^{-1} in the higher wave number region. The peak at 546 cm^{-1} may be identified as the AT48 mode of $\beta\text{-Al}_2\text{TiO}_5\text{-Al}_6\text{Ti}_2\text{O}_{13}$.

Fig. 3 presents the average micro-hardness of the AT40, AT48 single crystals and the polycrystalline AT40. The AT40 single crystal had a higher microhardness (10.79 GPa) than AT48 single crystal (9.88 GPa). It can be seen that a lower

mechanical data scatter is attained for the AT48, which is closely linked to the homogeneity of the microstructure. This may be attributed to the variation in microstructural differences, porosity and phase distribution. Although originally a pure Al₂O₃ single crystal exhibits a microhardness value of 11 GPa. The microhardness values of the Al₂O₃-40 wt.% TiO₂ are slightly higher than that of the Al₂O₃-48 wt.% TiO₂. It is shown that the microhardness values of depend on the amount of TiO₂.

The results of the scratch tests are seen in Fig. 4. The completion of the test cycle resulted in a wear track with a maximum depth of 9200 nm. Scratch testing is an appropriate technique that provides more fundamental information on wear mechanisms and is used to simulate the fracture in sliding wear. The normal load and its corresponding tangential force were recorded simultaneously during scratch tests. All test materials were scratched successively to identify the trend of tangential force with increased number of scratches at a constant maximum normal load. According to the scratch tests, neither crystal displayed fracture or crack advancement in the form of a cleavage plane. However, the line thickness and depth in the AT40 crystal were smaller (Fig. 4(b)). These results support the results of the microhardness assays that indicated that the AT40 had a higher hardness (10.79 GPa compared to 9.88 GPa). Single crystal ceramics generally have a high hardness since they do not contain grain boundaries or vitreous phases.

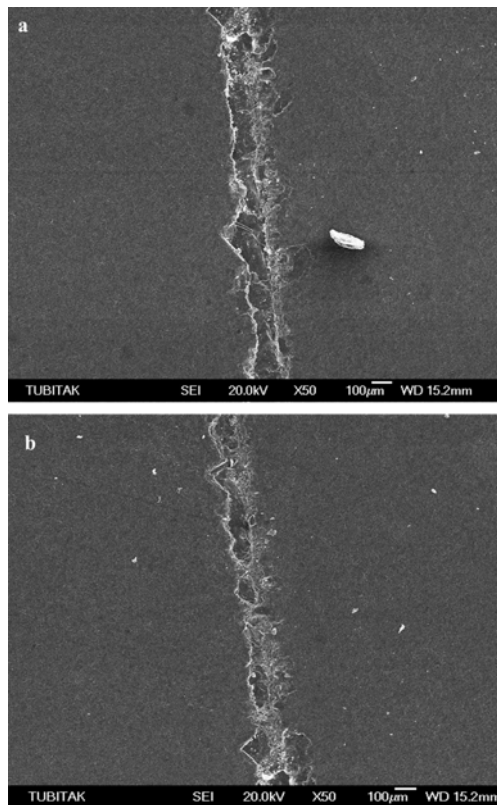


Fig. 4. Scratch tests conducted under identical conditions for the (a) AT48 single crystal (b) AT40 single crystal. Parameters of the scratch test: length; 10 mm, normal load; 30 N, loading rate; 5 N·minute⁻¹, speed; 2.5 mm·minute⁻¹, penetration depth; 9200 nm.

In Fig. 5, the surface topographies of the AT40 and the AT48 are shown. The AT40 and AT48 single crystals were cut with a diamond saw and were compared in terms of abrasion, friction and surface roughness. Hardness and brittleness are generally directly proportional in polycrystalline ceramics. However, as can be seen in Fig. 6, the nearly perfect smoothness of the AT48 indicates a lack of brittleness during cutting. The low roughness on the AT40 crystal similarly indicates a low brittleness. The AT40 single crystal has relatively smooth surfaces, with root mean square roughness values > 175 nm. One can note that the surface is rather rough and hillocky. The disposition of the hills appears to be random. However, there are surface areas with a periodic disposition of hills. AFM analysis data show that the native relief of AT48 is very rough and some periodicity in disposition of grains. The analogous in regularities, namely, the appearance of a periodical disposition of asperities on the surface of a crystal as a consequence of single crystal AT40 is the smoother relief and the lower values of roughness parameters in comparison with those for the similar type of single crystal AT48. We speculate that both are related to threading dislocations. Since this surface roughness is worse in thinner AT48 crystal, severe strain coming from thermal expansion coefficient differences may cause redistribution of dislocations at the interface

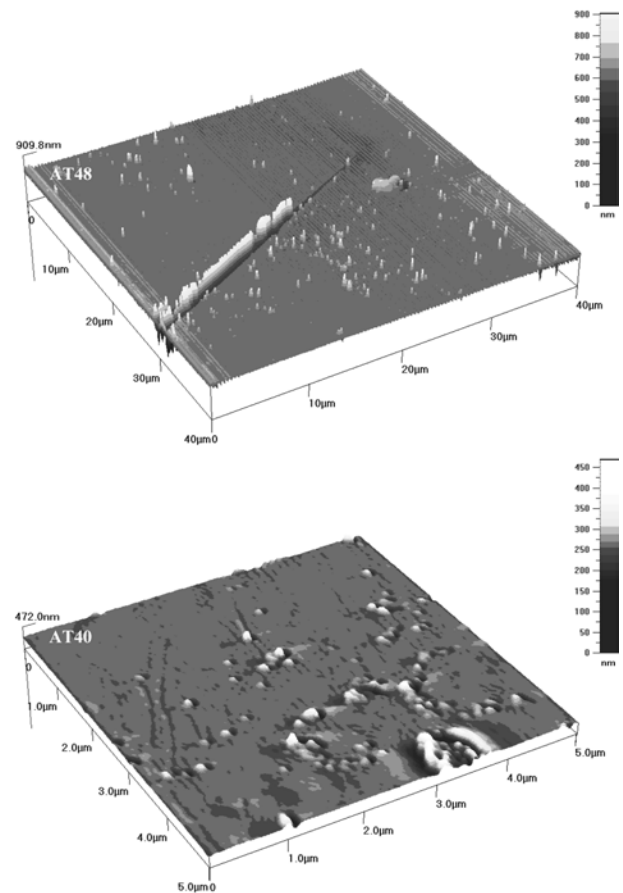


Fig. 5. AFM images of samples (a) AT48 and (b) AT40. The height scale relevant for each sample is indicated in nm.

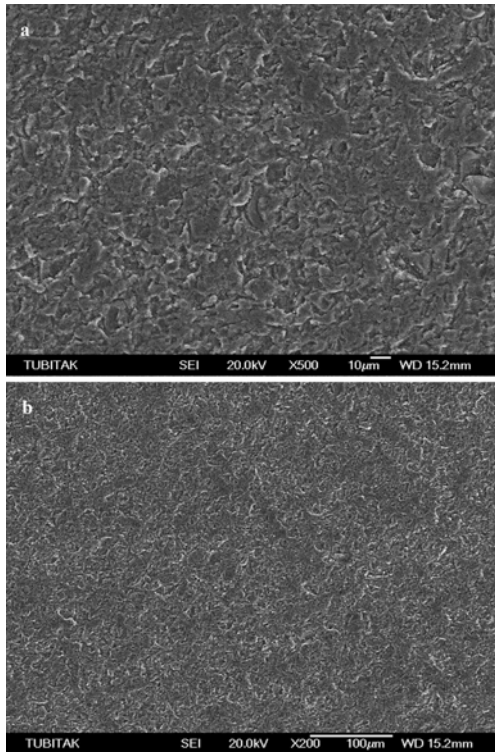


Fig. 6. (a) SEM micrograph of the AT40 single crystal. The light grey zones in the single crystal indicate Al_2TiO_5 , and the dark grey zones indicate Al_2O_3 phases. (b) SEM image of a longitudinal section of sample AT48 exhibiting dark dendrites in a bright matrix.

and in the AT48 during annealing and cooling, resulting in surface roughening on the thin AT48 crystal.

Eutectic composites are completely free of these microstructural factors, they show excellent creep characteristics. On the other hand, sintered composites have poor creep characteristics because they include grain boundaries and triple grain junctions with amorphous phases that are bad for high temperature creep [16]. Two separate phases without the grain boundaries are observed in Fig. 6(a), which shows the SEM image of an AT40 single crystal, confirming the presence of various phases without grain boundaries. The bright light grey areas indicate an Al_2TiO_5 phase, and the dark grey areas indicate an Al_2O_3 phase. The plain sample without an addition revealed a typical aluminium titanate microstructure, with a combination of unreacted Al_2O_3 and TiO_2 , pores and transgranular micro cracks through Al_2TiO_5 grains that occurred during cooling due to appreciable thermal expansion anisotropy of individual Al_2TiO_5 grains. The presence of pores in the solidified rods was one of the main concerns because of their influence on the mechanical properties in the SEM micrograph of Fig. 6(b) the bright phase in the AT48 crystal is 40% by weight alumina and the dark one is Al_2O_3 in the AT48 crystal the microstructure consists is rather inhomogeneous across the sample. In some places, the formation of coarser regions, similar to the onset of irregular colonies can be observed.

The dilatometric method may be applied to any phase transformation process, generating a dimensional change,

crystallisation are crystal phase transformation. It may be utilised if the variation connected to the above-mentioned transformation is sufficiently large for the sensitivity of the technique employed. The AT40 and AT48 single crystal thermal expansion behavior is shown in Table 1. The thermal expansion of the AT48 crystal is larger than the AT40 crystal because the tensions formed by the two phases in the AT48 crystal have very different expansion rates. The micro-cracks formed by this tension prevent the advance of large cracks that appear during shock or sudden temperature variations. These micro-cracks therefore reduce the disadvantage posed by a low shock resistance in oxide crystals.

Furthermore, the length of the crack in the eutectic will be restricted by the tortuous interfaces of and their orientation changes. Such a micro-cracked eutectic is expected to exhibit higher toughness but also lower strength if crack lengths exceed critical values of defect length. A balance between strength and toughness could be achieved by reinforcing the eutectic matrix by a continuous load-bearing phase with a larger strain to failure than the matrix. The examination of the Al_2O_3 - TiO_2 phase diagrams shows that the directional solidification from an alumina rich off eutectic melt should produce continuous Al_2O_3 primary dendrites separated by a Al_2TiO_5 - Al_2O_3 eutectic matrix. Weak interfaces are also expected to develop locally along interfaces between Al_2O_3 dendrites and the Al_2TiO_5 phase of eutectic [13]. These characteristics should provide an in situ composite with higher strength than the AT40 crystal and a failure mode comparable with those of AT48 crystal.

Fig. 7 shows typical stress displacement curves of four point flexural tests obtained at 1673 K from a specimen parallel to the solidification direction of the AT40, AT48

Table 1. Thermal expansion coefficient of AT40 and AT48 single crystals

AT40 single crystal, $\times 10^{-6}\text{K}^{-1}$			AT48 single crystal, $\times 10^{-6}\text{K}^{-1}$		
α_a 25-1000 °C	α_b 25-1000 °C	α_c 25-1000 °C	α_a 25-1000 °C	α_b 25-1000 °C	α_c 25-1000 °C
7.8	16.5	8.5	10.3	20.6	-2.4
α_a 1000-25 °C	α_b 1000-25 °C	α_c 1000-25 °C	α_a 1000-25 °C	α_b 1000-25 °C	α_c 1000-25 °C
9.7	22.4	11.8	14.3	26.5	-4.3

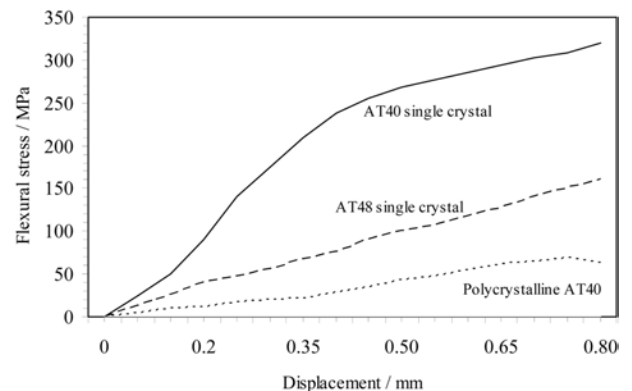


Fig. 7. Typical stress displacements of the AT40, AT48 crystals and polycrystalline AT40 obtained from four point flexural tests at 1400 °C.

crystals and polycrystalline AT40 large ingot (~250 g) with 38 mm diameter and 60 mm length. The samples shows strength are about respectively 320 MPa, 110 MPa and 85 MPa.

Conclusions

AT48 crystals have hardness, scratch resistance, surface roughness, properties. But negative results compared to AT40 crystals were obtained. Inclusions do not result in large decreases in these properties. The expansion behavior of the crystals shows that the AT40 single crystal has a mechanism for shock resistance during thermal fluctuations. Thus, the AT40 single crystal has an advantage over many eutectic single crystals, including sapphire, that display low shock resistance. Besides AT40 crystals have better bending strength the same composition as the polycrystalline and AT48 crystals.

Acknowledgements

I am grateful to Dr. Y. Nakazumi and Mr. T. Matsumoto of Nakazumi Crystal for their help in the experiments.

References

1. Y. Waku, N. Nakagawa, T. Wakamoto, H. Ohtsubo, K. Shimizu and Y. Kohtoku, *Nature*, 389 (1997) 49-52.
2. D. Viechnicki and F. Schmid, *J. Mater. Sci.* 4 (1969) 84-88.
3. F.L. Kennard, R.C. Bradt and V.S. Stubican, *J. Am. Ceram. Soc.* 59 (1976) 160-163.
4. B.M. Epelbaum, A. Yoshikawa, K. Shimamura, T. Fukuda, K. Suzuki and Y. Waku, *J. Cryst. Growth*, 198-199 (1999) 471-475.
5. J.M. Calderon-Moreno and M. Yoshimura, *Scripta Mater.* 44 (2001) 2153-2156.
6. A. Larrea, G.F. de la Fuente, R.I. Merino and V.M. Orera, *J. Eur. Ceram. Soc.* 22 (2002) 191-198.
7. I.M. Low, *Mater. Res. Bull.* 33 (1998) 1475-1482.
8. N.P. Padture, S.J. Bennisson and H.M. Chan, *J. Am. Ceram. Soc.* 76 (1993) 2312-2320.
9. J.F. Bartolomé, J. Requena, J.S. Moya, M. Li and F. Guiu, *Acta Mater.* 44 (1996) 1361-1370.
10. B.R. Lawn, in "Fracture of Brittle Solids" (Cambridge University Press, 1996) p.72-85, 202-206.
11. C. Baudin, A. Sayir and M.H. Berger, *Acta Mater.* 54 (2006) 3835-3841.
12. A. Sayir, M.H. Berger and C. Baudin, *Ceram Eng. Sci. Proc.* 26 (2005) 225-233.
13. M.H. Berger and A. Sayir, *J. Eur. Ceram. Soc.* 28 (2008) 2411-2419.
14. M. Goebbels and D. Bostroem, *Berichter der Deutschen Mineralogischen Gesellschaft*, 9 (1997) 128.
15. D. Goldberg, *Rev. Int. Hautes Temper. Refract.* 5 (1968) 181-194.
16. Y. Waku, N. Nakagawa, T. Wakamoto, H. Ohtsubo, K. Shimizu and Y. Kohtoku, *J. Mater. Sci.* 33 (1998) 1217.

1. Y. Waku, N. Nakagawa, T. Wakamoto, H. Ohtsubo, K.